Article

Molecular Structures and Dynamics of the Stepwise Activation Mechanism of a Matrix Metalloproteinase Zymogen: Challenging the Cysteine Switch Dogma

Gabriel Rosenblum, Samy Meroueh, Marta Toth, Jed F. Fisher, Rafael Fridman, Shahriar Mobashery, and Irit Sagi

J. Am. Chem. Soc., **2007**, 129 (44), 13566-13574• DOI: 10.1021/ja073941l • Publication Date (Web): 12 October 2007

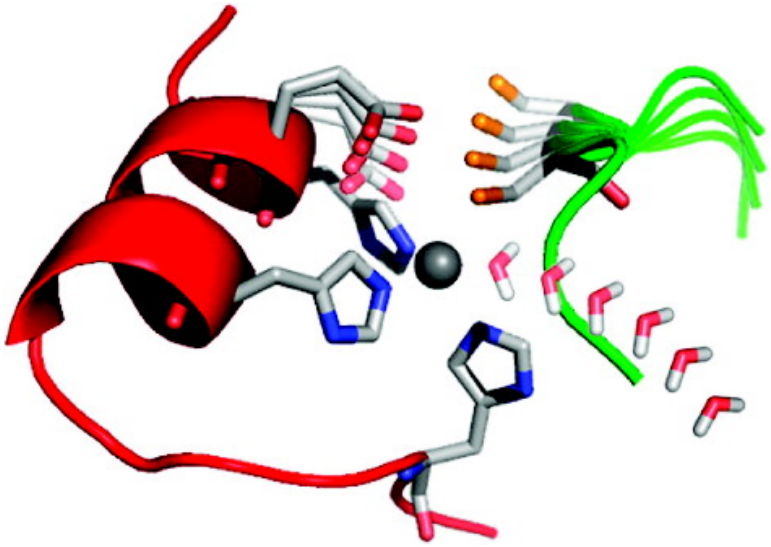

J|A|C|S
ARTICLES
Published on Web 10/12/2007

Molecular Structures and Dynamics of the Stepwise Activation Mechanism of a Matrix Metalloproteinase Zymogen: Challenging the Cysteine Switch Dogma

Gabriel Rosenblum,[†] Samy Meroueh,[‡] Marta Toth,[‡] Jed F. Fisher,[‡] Rafael Fridman,[§] Shahriar Mobashery,*[,‡] and Irit Sagi*[,†]

Contribution from the Department of Structural Biology, The Weizmann Institute of Science, Rehovot, 76100, Israel, Department of Chemistry and Biochemistry and Walther Cancer Research Center, University of Notre Dame, Notre Dame, Indiana, 46556, and Department of Pathology, Wayne State University, Detroit, Michigan 48202

Received May 31, 2007; E-mail: mobashery@nd.edu; irit.sagi@weizmann.ac.il

Abstract: Activation of matrix metalloproteinase zymogen (pro-MMP) is a vital homeostatic process, yet its molecular basis remains unresolved. Using stopped-flow X-ray spectroscopy of the active site zinc ion, we determined the temporal sequence of pro-MMP-9 activation catalyzed by tissue kallikrein protease in milliseconds to several minutes. The identity of three intermediates seen by X-ray spectroscopy was corroborated by molecular dynamics simulations and quantum mechanics/molecular mechanics calculations. The cysteine−zinc interaction that maintains enzyme latency is disrupted via active-site proton transfers that mediate transient metal−protein coordination events and eventual binding of water. Unexpectedly, these events ensue as a direct result of complexation of pro-MMP-9 and kallikrein and occur before proteolysis and eventual dissociation of the pro-peptide from the catalytic site. Here we demonstrate the synergism among long-range protein conformational transitions, local structural rearrangements, and fine atomic events in the process of zymogen activation.

Introduction

The matrix metalloproteinase (MMP) family of zinc proteases occupies a central role in the homeostatic regulation of the extracellular environment and of innate immunity.[1] Aberrant control of MMP activity contributes to diseases such as cancer, arthritis, asthma, stroke, and atherosclerosis (see ref 2 for references). Zymogen activation is a major mechanism for the cellular control of MMP activity.[3] Among the unresolved questions relating to MMP zymogen activation are the basis for its occurrence and the extent to which its elevation correlates to disease progression. Thus, the biochemical pathways involved in MMP zymogen activation and the molecular mechanism of the zymogen transformation are of intense interest.[4−8] All members of the human MMP family are synthesized as inactive zymogens containing an approximately 80 amino acid N-terminal pro-peptide domain that is adjacent to the zinc-containing catalytic domain.[9] The pro-peptide domain contains a "cysteine switch" PRCXXPD consensus sequence.[10] The cysteine in this sequence coordinates to the zinc ion of the zymogen (Figure 1A). MMP activity is suppressed as a result of zinc−cysteine coordination and pro-peptide domain occlusion of the active site. MMP zymogens (or pro-MMPs) are activated *in vivo* by proteases including tissue kallikrein, trypsin, and other MMPs[11] and *in vitro* by chemical agents such as aminophenyl mercuric acetate and other S-reactive agents, reactive oxygen, detergents, and heat.[10−12] Zymogen activation releases the pro-peptide domain by sequential proteolysis, mediated by physiological proteases.[10,11,13] The first proteolytic cleavage occurs in the loop connecting two helices of the pro-peptide, and the second cleavage occurs eight amino acid residues downstream from the zinc-coordinated cystein (Figure 1A, black arrows). Pioneering work by Nagase and co-workers invokes the importance of protein conformational transitions to the zymogen activation mechanism.[14]

The acquisition of MMP proteolytic activity is not necessarily coincident with these proteolytic cleavages, especially when using chemical agents. An early event in the mercurial activation

[†] The Weizmann Institute of Science.
[‡] University of Notre Dame.
[§] Wayne State University.

(1) Mott, J. D.; Werb, Z. *Curr. Opin. Cell Biol.* **2004**, *16*, 558−564.
(2) Overall, C.; Kleifeld, O. *Br. J. Cancer* **2006**, *94*, 941−946.
(3) Folgueras, A. R.; Pendás, A. M.; Sánchez, L. M.; López-Otín, C. *Int. J. Dev. Biol.* **2004**, *48*, 411−424.
(4) Stetler-Stevenson, W. *J. Clin. Invest.* **1999**, *103*, 1237−1241.
(5) Rao, J. *Nat. Rev. Cancer* **2003**, *3*, 489−501.
(6) Mook, O. R. F.; Frederiks, W. M.; Van Noorden, C. J. F. *Biochim. Biophys. Acta* **2004**, *1705*, 69−89.
(7) Chirco, R.; Liu, X.; Jung, K.; Kim, H. *Cancer Metastasis Rev.* **2006**, *25*, 99−113.
(8) Strongin, A. *Cancer Metastasis Rev.* **2006**, *25*, 87−98.
(9) Bode, W.; Maskos, K. *Biol. Chem.* **2003**, *384*, 863−872.
(10) Springman, E. B.; Angleton, E. L.; Birkedal-Hansen, H.; Van Wart, H. E. *Proc. Natl. Acad. Sci. U.S.A.* **1990**, *87*, 364−368.
(11) Nagase, H. *Biol. Chem.* **1997**, *378*, 151−160.
(12) Koklitis, P. A.; Murphy, G.; Sutton, C.; Angal, S. *Biochem. J.* **1991**, *276*, 217−221.
(13) Chen, L. C.; Noelken, M. E.; Nagase, H. *Biochemistry* **1993**, *32*, 10289−10295.
(14) Nagase, H.; Enghild, J. J.; Suzuki, K.; Salvesen, G. *Biochemistry* **1990**, *29*, 5783−5789.

10.1021/ja073941l CCC: $37.00

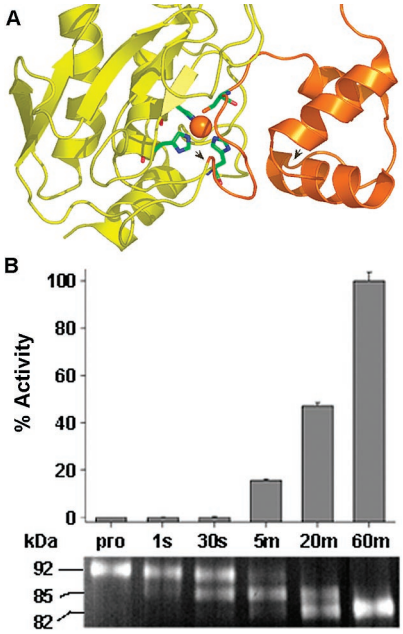

Figure 1. Activation of pro-MMP-9 by sequential proteolysis. (A) 3D structure of pro-MMP-9 shown in ribbon representation (PDB ID: 1L6J). The catalytic and the pro-peptide domains are shown in yellow and orange, respectively. The catalytic zinc ion is depicted as an orange sphere and bound to three conserved histidines and to the pro-peptide cysteine. The gray arrows indicate the Leu-Ser at positions 78−79 (right arrow) and Phe−Gln at positions 107−108 (left arrow) cleavage sites. (B) Lower panel: Time-dependent gel zymography analysis of pro-MMP-9 during activation by its activator tissue kallikrein. The reaction was quenched with SDS buffer at the indicated time points (see Materials and Methods). At $t = 0$, pro-MMP-9 is a single gel band at 92 kDa. The first cleavage of the pro-peptide occurs in the 1−30-s interval. The 85 kDa band that results from the first cleavage is distinct from that of the zymogen (see text). The fully activated enzyme (82 kDa) is detected at 5−60 min while its activity is enhanced with time. Upper panel: Kinetic assay of enzyme activity by fluorogenic peptide hydrolysis.[23] In agreement with the gel zymography assay, activity appears gradually during the 5−60-min interval.

of the MMP-3 zymogen is the appearance of proteolytic activity, without change in the molecular mass of the protein. Proteolytic processing to two lower molecular weight MMP proteins is subsequent.[15] A similar separation of these two events occurs in the *in vivo* activation of the MMP-9 zymogen by nitrous oxide during cerebral ischemia.[16] These observations indicate the existence of a mechanism for the displacement of the pro-peptide domain, with loss of the cysteine coordination, in the absence of pro-peptide domain proteolysis. One explanation is that during activation of MMP-1 and MMP-3, the first proteolytic cleavage destabilizes the pro-peptide domain conformation, disrupting the cysteine−zinc interaction and resulting in an active enzyme form.[14] *There is not, however, a single pro-MMP example where the sequential molecular events of the cysteine departure and the proteolytic processing are resolved.* This absence is now addressed for the MMP-9 zymogen in this report.

Materials and Methods

Protein Expression and Purification. Recombinant 92-kDa MMP-9 zymogen was purified from media of HeLa cells suspension cultures that were infected with recombinant vaccinia virus, encoding the full length cDNA of human pro-MMP-9 as described previously.[17] All reactions were carried out in buffer C that contained 50 mM Tris/HCl, pH 7.5, 5 mM $CaCl_2$, 150 mM NaCl, and 0.02% Brij-35. Protein concentrations were determined using the molar extinction coefficient of 114 360 M^{-1} cm^{-1}[18] and with protein assay kit (BCA, Pierce). Protein concentrations were verified by X-ray "edge step analysis" for MMP-9.[19] Gelatin zymography and SDS-PAGE were preformed to determine protein purity and integrity by standard procedures.[20,21]

Inductively Coupled Plasma-Atomic Emission Spectroscopy (ICP-AES). The metal content of pro-MMP-9 was analyzed by inductively coupled plasma atomic emission spectroscopy using the ICP-AES model "Spectroflame" from Spectro. The samples were digested with 5% nitric acid in metal-free water, and the volume was adjusted to 6 mL. The zinc content of the enzyme was determined relative to its equivalent protein concentration. The ICP-AES results were confirmed by X-ray absorption "edge step analysis". Both methods were consistent with 1:1 zinc/protein ratio as also reported before.[19]

Activation of pro-MMP-9 by Tissue Kallikrein. We used the trypsin-like enzyme tissue kallikrein from porcine pancreas (Sigma-Aldrich, K-3627) as MMP-9 zymogen activator.[22] Tissue kallikrein was prepared at a 0.3 mM concentration and pro-MMP-9 was prepared at 0.075 mM concentration such that the pro-MMP-9-to-kallikrein ratio of 1:4 was achieved upon mixing equal volumes of enzyme solutions. Solutions were prepared in buffer C supplemented with 20% glycerol. Following incubation for different time intervals, the reaction was chemically quenched by addition of phenylmethylsulphonyl fluoride (PMSF) to a final concentration of 10 mM. Full inhibition of tissue kallikrein was obtained at these conditions. MMP-9 activity (not affected by PMSF) was immediately measured using the fluorogenic substrate Mca-Pro-Leu-Gly-Leu-Dpa-Ala-Arg-NH_2 following a reported procedure.[23] Substrate hydrolysis was followed by measurement of the fluorescent intensity at λ_{ex} 340 nm and λ_{em} 390 nm,[24] using Spectrafluor Plus spectrophotometer (Tecan). In addition, the apparent molecular weight of the activated MMP-9 at different incubation times was monitored using gelatin zymography.

N-Terminal Protein Sequencing. MMP-9 zymogen (27.5 μg) was cleaved by tissue kallikrein in 6:1 molar ratio at 50-μL buffer C at 37 °C. Aliquots were taken from the reaction after 2 and 10 min and were mixed with 4X reducing Laemmli sample buffer[25] supplemented with protease inhibitor cocktail (Halt protease inhibitors, Pierce) to stop the reaction. The samples were subjected to 10% SDS-PAGE (7 μg of protein per lane), transferred to poly(vinylidene difluoride) (PVDF) membrane, and stained with 0.1% Coomassie Blue Brilliant R-250 in 1% acetic acid, 40% methanol. The corresponding bands were cut out from PVDF membrane and sent for N-terminus microsequencing to ProSeq.

Activation of pro-MMP-9 by Inhibited Tissue Kallikrein. In additional experiments, tissue kallikrein was incubated with 10 mM PMSF (final concentration). Activity assay showed that full inhibition of tissue kallikrein was achieved. Increasing amounts of the inhibited tissue kallikrein were incubated for 20 min with pro-MMP-9. The samples were then subjected to gelatin zymography and MMP-9 activity assay as described. Free tissue kallikrein was used at the same conditions as a reference.

(15) Okada, Y.; Harris, E. D., Jr.; Nagase, H. *Biochem. J.* **1988**, *254*, 731−741.
(16) Gu, Z.; Kaul, M.; Yan, B.; Kridel, S. J.; Cui, J.; Strongin, A.; Smith, J. W.; Liddington, R. C.; Lipton, S. A. *Science* **2002**, *297*, 1186−1190.
(17) Fridman, R.; Toth, M.; Pena, D.; Mobashery, S. *Cancer Res.* **1995**, *55*, 2548−2555.
(18) Murphy, G.; Willenbrock, F. *Methods Enzymol.* **1995**, *248*, 496−510.
(19) Kleifeld, O.; Van den Steen, P. E.; Frenkel, A.; Cheng, F.; Jiang, H. L.; Opdenakker, G.; Sagi, I. *J. Biol. Chem.* **2000**, *275*, 34335−34343.
(20) Sambook, J.; Fritsch, E. F.; Maniatis, T. *Molecular Cloning: A Laboratory Manual*, 2nd ed.; Cold Spring Harbor Laboratory Press: Cold Spring Harbor, NY, 1989.
(21) Brown, P. D.; Levy, A. T.; Margulies, I. M.; Liotta, L. A.; Stetler-Stevenson, W. G. *Cancer Res.* **1990**, *50*, 6184−6191.
(22) Desrivieres, S.; Lu, H.; Peyri, N.; Soria, C.; Legrand, Y.; Menashi, S. *J. Cell. Physiol.* **1993**, *157*, 587−593.
(23) Knight, C. G.; Willenbrock, F.; Murphy, G. *FEBS Lett.* **1992**, *296*, 263−266.
(24) Netzel-Arnett, S.; Mallya, S. K.; Nagase, H.; Birkedal-Hansen, H.; Van Wart, H. E. *Anal. Biochem.* **1991**, *195*, 86−92.
(25) Laemmli, U. K. *Nature* **1970**, *227*, 680−685.

Freeze−Quench Sample Preparation of Activated MMP-9. All samples for X-ray absorption spectroscopy (XAS) were prepared before data collection. Equal volumes of pro-MMP-9 and tissue kallikrein (at the same reaction conditions already mentioned) were rapidly mixed and frozen on copper sample holders ($10 \times 5 \times 0.5$ mm^3) covered with Mylar tape. Freezing was performed in an isopentane bath, where the sample was cooled with liquid nitrogen to a temperature of −130 °C. The aging times ranged from 0 (pro-form) to 1400 ms in 50−100-ms intervals. Active MMP-9 sample was prepared after a mixing period of 30 min. The frozen samples were immediately transferred to liquid nitrogen and maintained at this or lower temperature throughout the experiment.

XAS Data Collection. XAS data collection was performed at the National Synchrotron Light Source at Brookhaven National Laboratory, beamline X9B. The frozen samples were mounted inside a Displex closed-cycle helium cryostat, and the temperature was maintained at 14 K to minimize the thermal disorder in the XAS data. The spectra were recorded at the Zn *k*-edge in fluorescence geometry. The beam energy was defined using a flat Si(111) monochromator crystal. The incident beam intensity I_0 was recorded using an ionization chamber. The fluorescence intensity was recorded using a 13-element germanium detector (Canberra). The transmission signal from a zinc foil was measured with a reference ion chamber simultaneously with fluorescence to calibrate the beam energy. Five scans of each sample were collected above 1×10^6 counts across the edge. The samples were checked for burning marks after each scan, and the beam position on the sample was changed before each scan to minimize radiation damages.

XAS Data Processing and Analysis. The average Zn *k*-edge absorption coefficient μ(E), which was obtained after five independent XAS measurements for each sample, was aligned using the first inflection point of a reference Zn metal foil XAS data (9659 eV). Subsequently, the absorption coefficients for different samples were shifted in X-ray energy until their first inflection points were aligned at the same energy.

The smooth atomic background was removed with the AUTOBK program of the UWXAFS data analysis package.[26] The same energy, $E_0 = 9659$ eV, was chosen for the purpose of background removal as the origin of the photoelectron energy. After the removal of background, the useful *k*-range in the resultant $\chi(k)$ was set, according to noise level, to be between 2.0 and 9.0−10.5 Å^{-1}. Model data for the fitting procedure were constructed by extracting the catalytic zinc site coordinates from the crystallographic coordinates of gelatinase A (PDB ID: 1CK7, 1SLM[27,28]). Using the computer code FEFF7,[29,30] we calculated the theoretical photoelectron scattering amplitudes and phase shifts. Total theoretical $\chi(k)$ was constructed by adding the most important partial $\chi(k)$'s that contributed to the *R*-range of interest.

To quantitatively derive the local structure around the catalytic zinc ion of MMP-9 during the activation process, we applied the following extended X-ray absorption fine structure (EXAFS) analysis methods: principal component analysis (PCA) and residual phase analysis (RPA).[31]

PCA. Using PCA, it is in many cases possible to reveal (model independently) the number of different species represented in the sample without a priori knowledge of their identity. The collection of EXAFS spectra measured at different time points represents the data matrix of vectors in multidimensional space and can be treated by conventional linear algebra methods to obtain eigenvalues and eigenvectors. The change in decay slope of its eigenvalues arranged in descending order (the "scree test") allows obtaining the number of principal components that dominate the data. To further examine the validity of the computed number of components, a restoration of the data set by a linear combination of the dominating spectral components was carried.

RPA. On the basis of our principal component analysis, we assumed that the EXAFS spectra at the various time points result from two main constituents, namely the starting (known) component of pro-MMP-9 and an intermediate complex of unknown structure. Therefore, the experimental EXAFS data can be written as:

$$\chi_D^{ex}(k) = x\chi_S^{ex}(k) + (1 - x)\chi_R(k) \quad (1)$$

where the first term on the right-hand side of eq 1 describes EXAFS from the starting phase, which will be subtracted from the total signal. The second term denotes EXAFS originating from the residual phase only. The weighting coefficient *x* in eq 1 is the actual (species) mixing fraction to be determined by this method. The coordination number, metal−ligand bond distances, and the Debye−Waller factors of each time-dependent spectrum were analyzed by iteratively subtracting different ratios (from 0 to 100%) of the known EXAFS spectrum of pro-MMP-9 (i.e., the starting phase) and fitting the residual spectrum to theoretical amplitudes and phases calculated by means of FEFF7.[29,30]

The EXAFS spectra were first subjected to multiple dataset fits.[31] In this analysis, the whole data set (17 spectra) was simultaneously fitted to the theoretical model calculated using FEFF7 (see Supporting Information).[29] This analysis provided the initial information about changes in coordination number and ligand identity that resides above the noise level. Individual spectra were then subjected to a more refined data analysis procedure.

The individual residual spectra were analyzed by an automated manner[31] using FEFFIT[26] fitting analysis. This script automatically fitted the residual fraction of the data and accounted for a number of models, each with different number and identity of ligands. All results were sorted, and the best fits were used as a lead to a manual fitting refinement.

Protein−Protein Docking. The initial complex between pro-MMP-9 and tissue kallikrein was examined using the protein−protein docking package 3D-Dock.[32−34] The crystal structures used for docking were PDB ID 1L6J for pro-MMP-9[35] and PDB ID 1HIA for tissue kallikrein.[36] The crystal structure of the tissue kallikrein was confined to a monomer, while the hirustasin inhibitor was excluded. This yielded the free enzyme in the bound conformation. A global scan of rotational and translational space was preformed using Fourier transform, while the grid spacing was 0.7 Å. The output complexes were ranked according to surface complementarities and electrostatic characteristics. As shape complementarity is not sufficient to discriminate between large numbers of docked complexes, the structures resulting from the global search were reranked with empirically derived potential using the static likelihood of residue−residue contacts across the interface of the complexes. Finally, biochemical and structural knowledge was used to filter solutions; complexes were discarded if no pro-MMP-9 cleavage site (Leu-Ser at positions 78−79) was within 15 Å from the catalytic triad of the tissue kallikrein. The remaining solutions were subjected to rigid body refinement and side-chain rotamer optimization by using the program MULTIDOCK.[33] The refined solutions were then

(26) Stern, E. A.; Newville, M.; Ravel, B.; Haskel, D.; Yacoby, Y. *Physica B* **1995**, *208/209*, 117−122.
(27) Becker, J. W.; Marcy, A. I.; Rokosz, L. L.; Axel, M. G.; Burbaum, J. J.; Fitzgerald, P. M.; Cameron, P. M.; Esser, C. K.; Hagmann, W. K.; Hermes, J. D.; Springer, J. P. *Protein Sci.* **1995**, *4*, 1966−1976.
(28) Morgunova, E.; Tuuttila, A.; Bergmann, U.; Isupov, M.; Lindqvist, Y.; Schneider, G.; Tryggvason, K. *Science* **1999**, *284*, 1667−1670.
(29) Rehr, J. J.; Mustre de Leon, J.; Zabinsky, S. I.; Albers, R. C. *J. Am. Chem. Soc.* **1991**, *113*, 5135−5138.
(30) Zabinsky, S. I.; Rehr, J. J.; Ankudinov, A.; Albers, R. C.; Eller, M. J. *Phys. Rev. B: Condens. Matter* **1995**, *52*, 2995−3009.
(31) Frenkel, A. I.; Kleifeld, O.; Wasserman, S. R.; Sagi, I. *J. Chem. Phys.* **2002**, *116*, 9449−9456.
(32) Moont, G.; Gabb, H. A.; Sternberg, M. J. *Proteins: Struct., Funct., Genet.* **1999**, *35*, 364−373.
(33) Jackson, R. M.; Gabb, H. A.; Sternberg, M. J. *J. Mol. Biol.* **1998**, *276*, 265−285.
(34) Gabb, H. A.; Jackson, R. M.; Sternberg, M. J. *J. Mol. Biol.* **1997**, *272*, 106−120.
(35) Elkins, P. A.; Ho, Y. S.; Smith, W. W.; Janson, C. A.; D'Alessio, K. J.; McQueney, M. S.; Cummings, M. D.; Romanic, A. M. *Acta Crystallogr., Sect. D* **2002**, *58*, 1182−1192.
(36) Mittl, P. R.; Di Marco, S.; Fendrich, G.; Pohlig, G.; Heim, J.; Sommerhoff, C.; Fritz, H.; Priestle, J. P.; Grutter, M. G. *Structure* **1997**, *5*, 253−264.

compared to test for converging solutions. If a group of solutions exhibit rmsd of less than 1.5 Å, only the highly scored solution within this group was kept. The remaining complexes were than ranked according to the minimized energy value obtained by MULTIDOCK.

Computational Procedures. The crystal structure of pro-MMP-9[35] was used as a starting point for all calculations (PDB ID: 1L6J). Molecular dynamics (MD) simulations were carried out with the Sander module of the AMBER8 suite of programs.[37] Force field parameters for the protein were obtained from the Parm99 set of parameters, which is distributed along with AMBER8.[37] Atomic charges for protein residues were obtained from the Amber force field.[38] Atomic charge of active-site zinc ion was computed using the restrained electrostatic potential[39] methodology by carrying out a geometry optimization of Zn(II) bound to three imidazole rings that would mimic the histidine residues in the active site, followed by fitting of the electrostatic potential, which was done by the antechamber module of the AMBER8 package. A bonded model for Zn(II) was followed in this study, as reported earlier.[40] The system was immersed in a box of TIP3P waters,[41] such that no atom in the protein was less than 12 Å from any edge of the box. All bonds involving hydrogen atoms were constrained using the SHAKE algorithm.[42] Particle mesh Ewald was used to treat long-range electrostatics. Before any MD simulation, the system was equilibrated using the following procedure. First, the protein was held fixed with Cartesian restraints while the water molecules were energy-minimized with 1000 steps of steepest descent energy minimization and 50 000 steps of conjugate gradient energy minimization. A short MD simulation was then carried out by holding the protein fixed to enable water molecules to equilibrate around the protein. The restraints on the protein were gradually relaxed through a series of five energy minimizations with Cartesian restrains of 500, 100, 50, 10, 5, and 0 kcal/mol.[2] The system was then gradually warmed to 100 K for 100 ps, followed by another warming to 200 K over 100 ps. A final warming was carried out to 300 K over 100 ps, followed by isobaric MD simulation.

The two-layer ONIOM method with electrostatic embedding was used for mixed quantum mechanics/molecular mechanics (QM/MM) geometry optimization using the Gaussian03 package.[63] These calculations were carried out starting with structures that were collected from MD simulations. First, the systems were subjected to 50 000 steps of conjugate gradient energy minimization with the AMBER8 package. The program GaussView 3.04 was then used to assign the region that would be treated with quantum mechanics and the region that would be included in the molecular mechanics layer. The molecular mechanics region was treated with the Amber force field. The quantum region was treated with the SVWN/SDD level of theory, which was shown earlier to perform very well for zinc-coordinated thiol-containing compounds.[43]

Results and Discussion

Tissue Kallikrein Activates pro-MMP-9 by Sequential Proteolysis of the pro-Peptide. Tissue kallikrein, a serine protease, was used as the catalyst for pro-MMP-9 activation.[22] The time-dependent change in pro-MMP-9 molecular mass upon reaction with kallikrein (in a 4:1 kallikrein/zymogen molar ratio) was evaluated by gel electrophoresis and N-terminal sequencing (see Materials and Methods and Supporting Information). Proteolytic cleavage of pro-MMP-9 by tissue kallikrein occurs in two steps. The first proteolysis occurs between Leu-Ser at positions 78−79. The second proteolysis, separating the pro-peptide domain from the catalytic domain, occurs at Phe-Gln positions 107−108. These two protein products, having respective molecular masses of 85 and 82 kDa, are distinguished from the zymogen by SDS-PAGE gel-based analysis (Figure 1B and Supporting Information Figure S1).

The time dependency of this proteolysis was determined. Figure 1B shows the percentage of MMP-9 proteolysis as a function of time (upper panel) and the complementary time-dependent zymography (activity gel-based, lower panel) assay for pro-MMP-9 activation by tissue kallikrein. The initiation of the first Leu-Ser (positions 78−79) proteolysis is detected by zymography at 1 s. This is observed by a relatively weak zymography band at 85 kDa. At a reaction time of 5 min, the 85 kDa protein corresponding to the first protein product (MMP-9) is the major constituent (>90%). However, the total protease activity at 5 min is only 18% of the activity measured at 60 min. As the progressive increase in total activity from 5 to 60 min occurs with change in the molecular mass of the protein, *we conclude that the proteolyzed pro-peptide Ser-Phe at positions 79−107 dissociates from MMP-9 core domain to allow substrate access to the active site* (Figure 1B). These observations reveal neither the time frame nor the nature of the coordination changes at the zinc ion that accompany these changes.

Crystallographic studies of pro-MMP-9 and other MMP proteins show two Zn(II) atoms.[35] One is structural, and its ligand environment is unaltered by zymogen proteolysis. The second is the catalytic zinc ion. Quantitative analyses of the zinc stoichiometry in MMPs in solution have been of interest.[44−46] Measurements of the zinc ion content in various MMPs show variations between 1 and 2 equivalent of metal ions per protein molecule. Studies by Willenbrock et al.,[47] Springman et al.,[48] and Kleifeld et al.[19] demonstrate that the full-length MMP-9, as well as other MMPs, contains a single zinc ion. It has been suggested that the zinc content in MMPs might be dependent on the procedure for enzyme purification.[19,48] Therefore, we have quantified the zinc content in our protein samples before structural X-ray analyses. The zinc content in our protein preparation has been determined by ICP-AES and XAS (using edge step analysis; see Materials and Methods and ref 19). The ICP-AES analysis gave a zinc stoichiometry of 0.97 ± 0.04 zinc ions per protein molecule. This value is in excellent agreement with our X-ray absorption edge step analysis of 1.01 ± 0.14 zinc ions per protein molecule.

In pro-MMPs, the catalytic zinc ion is tetrahedrally coordinated by the conserved cysteine (Cys-99) and by three histidines. An additional characteristic is a cross-strand Cys-99 to Glu-402 hydrogen bond (O···S separation of 2.95 Å). Tetrahedral

(37) Case, D. A.; et al. *AMBER7*; University of California: San Francisco, CA, 2002.
(38) Cornell, W. D.; Cieplak, P.; Bayly, C. I.; Gould, I. R.; Merz, K. M.; Ferguson, D. M.; Spellmeyer, D. C.; Fox, T.; Caldwell, J. W.; Kollman, P. A. *J. Am. Chem. Soc.* **1995**, *117*, 5179−5197.
(39) Darden, T.; York, D.; Pedersen, L. *J. Chem. Phys.* **1993**, *98*, 10089−10092.
(40) Hoops, S. C.; Anderson, K. W.; Merz, K. M. *J. Am. Chem. Soc.* **1991**, *113*, 8262−8270.
(41) Jorgensen, W. L.; Chandraseklar, J.; Maduar, J. D.; Impey, R. W.; Klein, M. L. *J. Chem. Phys.* **1983**, *79*, 926−935.
(42) Ryckaert, J. P.; Ciccotti, G.; Berendsen, H. J. C. *J. Comput. Phys.* **1977**, *23*, 327−341.
(43) Acharya, M. R.; Venitz, J.; Figg, W. D.; Sparreboom, A. *Drug Resist. Updates* **2004**, *7*, 195−208.
(44) Crabbe, T.; Willenbrock, F.; Eaton, D.; Hynds, P.; Carne, A. F.; Murphy, G.; Docherty, A. J. *Biochemistry* **1992**, *31*, 8500−8507.
(45) Lowry, C. L.; McGeehan, G.; Le Vine, H., III. *Proteins: Struct., Funct., Genet.* **1992**, *12*, 42−48.
(46) Salowe, S. P.; Marcy, A. I.; Cuca, G. C.; Smith, C. K.; Kopka, I. E.; Hagmann, W. K.; Hermes, J. D. *Biochemistry* **1992**, *31*, 4535−4540.
(47) Willenbrock, F.; Murphy, G.; Phillips, I. R.; Brocklehurst, K. *FEBS Lett.* **1995**, *358*, 189−192.
(48) Springman, E. B.; Nagase, H.; Birkedal-Hansen, H.; Van Wart, H. E. *Biochemistry* **1995**, *34*, 15713−15720.

zinc coordination is also found in the active MMP, but with water now replacing the cysteine ligand. As the ligand structure of this zinc ion undergoes dramatic alteration during zymogen activation, a spectroscopic method that allows the time-dependent examination of the zinc−ligand coordination structure is uniquely suited to the study of zymogen transformation. We have used stopped-flow freeze−quench XAS to diagnose intermediary metal−protein species along the reaction pathways of metalloenzyme reactions.[31,49−52] XAS evaluates the ligand environment of the nearest coordination shell of the protein-bound metal ion and additionally the metal electronic structure.[29,53,54]

Structural Characterization of Trapped Zinc−Protein Species during Zymogen Activation. The identical reaction of pro-MMP-9 with tissue kallikrein was evaluated by stopped-flow freeze−quench XAS at intervals between 0 and 1400 ms and additionally at 2, 15, and 30 min (Figure 2). On the basis of our gel-based analysis (Figure 1B), we determined that the time intervals between 0 and 1400 ms represent the early stages of the activation reaction (first proteolytic cleavage), while the additional time points represent proteolytic intermediates during the activation reaction. The local structure of the catalytic zinc−protein complex was examined in the various samples generated at the selected time points. The X-ray absorption coefficient data at each time point were collected at the zinc K-edge. Figure 2B shows the fluorescence XAS data collected within 0−1400-ms time interval. The data, presented in the form of Fourier transform (FT) spectra, provide the radial distribution of the various atoms within the first and second coordination shells of the catalytic zinc ion in MMP-9. Apparent changes in the radial distribution spectra of the various time domains can be observed in the contour FT map between 0 and 1400 ms (Figure 2B). These spectral changes indicate that the local environment of the catalytic zinc ion undergoes structural transformations. The shape and amplitude of the FT peaks are directly related to the type and number of the amino acid residues that are bound to the zinc ion. Very small spectral change occurs beyond 1400 ms. Hence, the catalytic zinc ion achieves a stable ligand configuration, indistinguishable from that of the active enzyme, within 1400 ms. Remarkably, this time interval is much more rapid than either proteolytic event as detected by our gel-based analysis (Figure 1B).

Relative changes in the effective charge of the zinc ion were analyzed by monitoring the shifts in edge energy of the raw XAS data at the spectral edge region (the first inflection point in the spectrum). Spectral edge shifts were calibrated against zinc foil XAS spectra that were measured simultaneously. Significant changes in the total effective charge of the catalytic zinc ion are detected during 0−1400 ms (Figure 2C histogram). Local charge transitions may indicate transformations within the nearest coordination environment of the zinc ion.[49] Importantly, all of these transformations occur within the bimolecular tissue kallikrein−zymogen complex and before the first proteolysis. Three zinc−protein intermediates, designated as **I-1**, **I-2**, and **I-3**, are seen between the starting zymogen ($t = 0$ ms) and the zinc coordination of the mature enzyme ($t = 1400$ ms). These same intermediates are also observed in the radial distribution function of the raw EXAFS data as presented by the FT spectra of the various time points (Figure 2B). Increase in the first FT peak intensity may be correlated with change in coordination number. Specifically, an abrupt increase in the first-

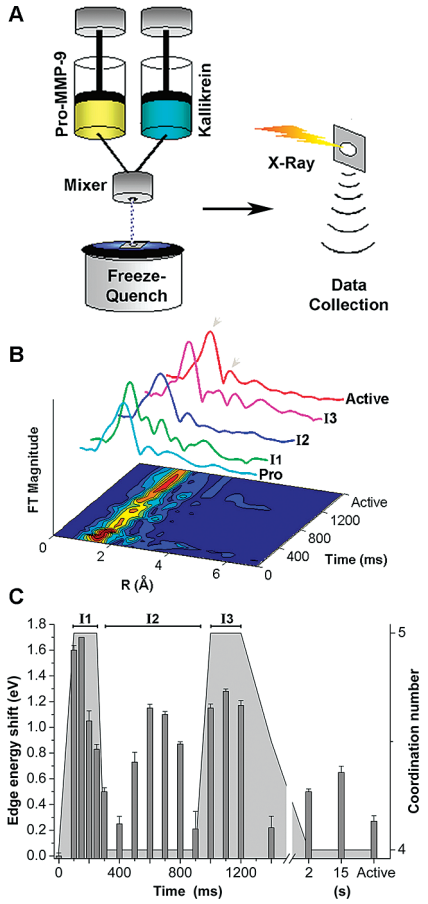

Figure 2. Time-resolved freeze−quench XAS of pro-MMP-9 during activation by tissue kallikrein. We chose a serine protease and not metalloproteinase (e.g., MMP-3) as zymogen activator to avoid the complication of introducing other active zinc−protein XAS spectral contributions to the data. Data were collected at the zinc K-edge between 0 and 1400 ms every 50−100 ms. Three additional time points were collected at 2 s, 15 s, and the fully active MMP-9 at 30 min. (A) Schematic representation of the experimental setup. The activation process was monitored at various time points where pro-MMP-9 was rapidly mixed with tissue kallikrein using stopped-flow apparatus equipped with a freeze−quench device.[19] Each time point is a sample quenched by rapid freezing in a liquid N_2-cooled isopentane bath. (B) Fourier-transformed spectra of the various time points represented by an artificially colored contour map. Red to blue represents high to low peak intensities. Individual spectra are shown for pro-MMP-9, **I-1**, **I-2**, **I-3**, and active MMP-9. The first and second peak intensities (gray arrows) of the various time domains represent the nearest coordination environment at the catalytic zinc site. Significant changes in the first-shell peak are detected for the different transient complexes. Specifically, the transition from a tetrahedral active-site zinc complex to a pentacoordinated zinc complex results in increased peak intensity. (C) Variation in absolute edge energy position during pro-MMP-9 activation as a function of time (left *y*-axis). The edge positions of the absolutely aligned XAS data were determined according to the maximum of the first derivative of each spectrum. Shifts in edge energy are represented in the histogram plot. Overall shifts to high and low energy are correlated with structural transitions of the catalytic zinc complex from pro-MMP-9 to **I-1**, **I-2**, and **I-3**. Changes in the total coordination number (right *y*-axis) of the zinc ion as represented by gray block graph.

(49) Kleifeld, O.; Frenkel, A.; Martin, J.; Sagi, I. *Nat. Struct. Biol.* **2003**, *10*, 98−103.
(50) Hwang, J.; Krebs, C.; Huynh, B. H.; Edmondson, D. E.; Theil, E. C.; Penner-Hahn, J. E. *Science* **2000**, *287*, 122−125.
(51) Lee, S. K.; George, S. D.; Antholine, W. E.; Hedman, B.; Hodgson, K. O.; Solomon, E. I. *J. Am. Chem. Soc.* **2002**, *124*, 6180−6193.
(52) Riggs-Gelasco, P. J.; Shu, L. J.; Chen, S. X.; Burdi, D.; Huynh, B. H.; Que, L.; Stubbe, J. *J. Am. Chem. Soc.* **1998**, *120*, 849−860.
(53) Scott, R. A. *Methods Enzymol.* **1985**, *117*, 414−458.
(54) Strange, R. W.; Hasnain, S. S. *Methods Mol. Biol.* **2005**, *305*, 167−196.

Table 1. Nonlinear Curve Fitting EXAFS Data Analysis Parameters of Zinc−Protein Ligand Intermediates during pro-MMP-9 Activation[a]

	3 × Zn-N/O-I		1 × Zn-S		1 × Zn-N/O-II		1 × Zn-N/O-III	
time (ms)	R (Å)	σ^2 (Å^2)	R (Å)	σ^2 (Å^2)	R (Å)	σ^2 (Å^2)	R (Å)	σ^2 (Å^2)
0 (pro)	1.93(1)	4.40×10^{-3}	2.26(4)	4.00×10^{-4}				
100	2.04(1)	2.80×10^{-3}	2.24(2)	3.50×10^{-4}	2.04(1)	2.80×10^{-3}		
150	1.90(1)	2.00×10^{-3}	2.25(2)	1.20×10^{-3}	1.90(1)	2.00×10^{-3}		
200	2.03(3)	5.20×10^{-3}	2.30(4)	3.70×10^{-3}	2.03(3)	5.20×10^{-3}		
250[b]	2.01(1)	3.50×10^{-3}	2.31(2)	4.70×10^{-3}	1.99(1)	3.50×10^{-3}		
300	2.00(1)	3.00×10^{-3}			1.99(1)	3.00×10^{-3}		
400	2.20(1)	4.20×10^{-3}			1.96(1)	9.00×10^{-4}		
500	2.05(1)	1.30×10^{-4}			1.90(3)	1.30×10^{-4}		
600	1.94(1)	1.00×10^{-3}			2.08(1)	1.00×10^{-3}		
700	1.97(1)	2.10×10^{-3}			1.80(1)	1.00×10^{-3} [c]		
800	2.01(1)	2.00×10^{-3}			1.83(2)	2.00×10^{-3}		
900	1.93(1)	4.90×10^{-3}			1.93(1)	4.90×10^{-3}		
1000	2.01(1)	2.00×10^{-3}			1.99(1)	2.00×10^{-3}	2.19(2)	1.00×10^{-3}
1100	1.95(7)	2.00×10^{-3}			2.06(4)	2.00×10^{-3}	1.95(7)	2.00×10^{-3}
1200	2.03(1)	1.70×10^{-3}			2.02(1)	1.70×10^{-3}	2.02(1)	1.70×10^{-3}
1400[b]	2.13(2)	7.00×10^{-4}			1.96(5)	5.00×10^{-3} [c]		
active	2.02(1)	1.00×10^{-3}			1.89(1)	1.00×10^{-3}		

[a] Nonlinear curve-fitting EXAFS data analysis parameters of zinc−protein ligand intermediates during pro-MMP-9 activation. The raw EXAFS spectra were processed and analyzed following reported procedures.[31] The various parameters were varied and fixed to examine the stability of each fit (for detailed analysis, see Supporting Information). The E_0 shifts were varied and fixed after optimization between the values of 8 to −8 eV (not shown).The fits are of the residual spectra resulting from iterative subtractions of fractions of the starting phases (pro-MMP-9) where R is the zinc−ligand bond distance in angstroms and σ^2 is the Debye−Waller factor. The first pentacoordinated intermediate (**I-1**) is detected at 100−250 ms, and the second pentacoordinated intermediate (**I-3**) is detected at 1000−1200 ms. The distances and Debye−Waller factors were guessed. [b] Inconclusive fit, in terms of the number of coordinated ligands, was obtained for the designated time points. The error in the last digit is given in parentheses. [c] Fixed parameter in the fit.

shell peak intensity is observed for **I-1** between 100 and 250 ms. This change is followed by a decrease in peak intensity for **I-2** between 300 and 900 ms, a further increase of the first-shell peak intensity for **I-3** between 1000 and 1200 ms, and a final decay to the active species.

The progressive changes in the zinc coordination were interpreted by combination of component analysis, multiple dataset fits, and residual phase analysis (see also Supporting Information).[31,49] These analyses resolve the zinc−protein bond distances, the number of different species in the zinc coordination, the nature of the coordinated species, and the mixing fractions of these species distinct by their spectra within the various trapped complexes (see Materials and Methods and Supporting Information). The coordination number, metal−ligand bond distances, and the Debye−Waller factors (indicator parameters for thermal disorder) for each spectrum were refined by iteratively subtracting different fractions of zinc−protein spectral contribution (from 0 to 60%) of the known XAS spectrum of pro-MMP-9 and fitting the residual spectrum to theoretical amplitudes and phases calculated by FEFF7.[29] Detailed spectral analyses are reported in the Supporting Information.

These analyses indicate that *both* the coordination numbers and distance parameters of the catalytic zinc ion in the MMP-9 zymogen undergo progressive change between 0−1400 ms (Table 1 and Figure 2C). The zinc ion in the zymogen has tetrahedral coordination by three O or N ligands (the XAS data do not distinguish between O and N spectral contributions) at 1.93 Å and one S ligand at 2.26 Å. These values agree fully with the tetrahedral zinc (having His-401, His-405, His-411, and Cys-99 ligands) seen in the MMP-9 zymogen crystal structure.[35] The association of tissue kallikrein to the zymogen is a reasonable basis for the change observed in the first 100 ms. In this interval, the tetrahedral zinc ion of the zymogen (detected at time = 0) converts to a pentacoordinated zinc by an additional Zn−N/O contribution, designated as intermediate-1 (**I-1**, Figure 2C and Table 1). The pentacoordinated zinc of **I-1** has one Zn−S (Cys-99) at 2.27 Å and four Zn−N/O at 1.98 Å. Transformation of **I-1** to **I-2** occurs by the decay of the Zn−S spectral contribution during the 300−900-ms interval. The zinc coordination in **I-2** is tetrahedral, with three Zn−N/O (His) at 2.01 Å and one Zn−N/O at 1.94 Å. The absence of sulfur in the zinc coordination sphere indicates dissociation of the "cysteine switch" and its replacement by a (presumably) oxygen ligand. **I-2** transforms to a second pentacoordinated species (**I-3**) over the 1000−1200-ms interval. The zinc coordination in **I-3** is consistent with four Zn−N/O contributions at average distance of 2.0 Å and one Zn−N/O at 2.19 Å. Last, the system evolves in the final 1400 ms to 15 min interval to that of the tetrahedral zinc species of the active MMP, with four Zn−N/O contributions at average distance of 1.99 Å. These distances agree with spectroscopic data.[19] As emphasized earlier, while the zinc coordination has matured, the MMP is not yet capable of catalysis (Figure 1B). It is important to note that the detected fluctuations in bond distances are within the limit of the X-ray data resolution (0.2 Å).

Figure 2C shows that identical kinetics for zymogen transformation to **I-1**, **I-2**, **I-3** and the final zinc structure are obtained by each method of data analysis. Transformation of the zinc−protein complex from tetracoordinated to pentacoordinate geometries is accompanied by abrupt transient change in the total effective charge of the zinc ion as the zymogen transforms through intermediates **I-1**, **I-2**, and **I-3** to the active zinc ion coordination structure. A shift to higher energy indicates greater effective positive charge on the zinc ion within the coordination sphere. Although zinc ions are generally not subject to substantive changes in their total effective charge, we reported previously that formation of a pentacoordinated zinc−protein intermediate, detected in solution in real time, increases the zinc partial positive charge.[49] Our results demonstrate that the transformation of the MMP-9 zymogen to the active MMP occurs by dynamic interconversions of pentacoordinated and tetracoordinated zinc precursors to facilitate the dissociation of the zinc−Cys bond. In addition, significant changes in local

effective charge of the zinc ion are observed during the lifetime of each intermediate complex while the structure is maintained. This implies that other protein dynamical events that cannot be resolved by this spectral analysis take place at the catalytic zinc site.

Our results clearly indicate the time frame for zinc−Cys dissociation without the requirement of proteolytic cleavage. This dissociation event gives rise to **I-2**, followed by the formation of **I-3**. Correlation of the conversion of **I-3** to the active zinc−protein complex with the attendant proteolysis of the pro-domain is more difficult to assign. Our results indicate that conversion of **I-3** to the active coordination sphere occurs beyond the 1.4 s time frame. Our gel-based analysis indicates that the process of the first cleavage of pro-MMP-9 by tissue kallikrein commences at about 1 s and proceeds to completion in the ensuing 5 min. This might suggest that the first cleavage event promotes conversion of **I-3** to the active form of MMP-9. Yet, we cannot rule out other possible scenarios that might take place at this stage, such as a process in which the conversion to the active form would not depend on the cleavage of the pro-peptide. Hence, activation of the pro-MMP-9 might actually happen before the proteolytic events.

Computational Analysis of Active-Site Dynamics and Structural Kinetics. These experimental results describe for the first time zymogen activation in terms of the catalytic zinc machinery along the activation pathway (Table 1). To clarify the intermediate structures, the computational methods of explicit solvent MD simulations and mixed QM/MM calculations were used (see Materials and Methods). A total of 75 ns of MD simulations were collected over 10 independent trajectories. Data analysis revealed that one trajectory captured the entire activation event, sampling conformers similar to those reported by the XAS experiment (see MPEG animation in Supporting Information video 1), whereas the remaining nine trajectories did not progress beyond the pro-MMP species. To provide quantitative agreement with experiment, snapshots from the MD simulation showing the activation event were subjected to QM/MM geometry optimization, whereby the residues coordinated to the zinc ion were treated at the QM level, while the remaining active-site residues were treated at the MM level. The starting structure for the calculations is the 2.5 Å resolution crystal structure (PDB ID: 1L6J) of pro-MMP9.[35] The atoms included in the pro-MMP-9 QM layer were the ligand side chains (His-401, His-405, His-411, Cys-99), the Glu-402 side chain (which is hydrogen-bonded to Cys-99 in the zymogen), and the catalytic zinc ion. Computational entry of this structure was made with the presumption of standard ionizations to the Cys-99-Glu-402 hydrogen bond (that is, a neutral thiol and a carboxylate anion).[55] However, during QM/MM geometry optimization, a quite unexpected proton migration occurred from the Cys-99 thiol to the Glu-402 carboxylate (Figure 3A and MPEG animation in Supporting Information video 1). This indicates that Cys-99 is a *thiolate* zinc ligand in the MMP-9 zymogen. The Zn−S (2.24 Å) and Zn−N (mean 1.95 Å) bond lengths in the QM/MM geometry-optimized structure for the pro-MMP-9 agree to within <0.1 Å of the XAS values (Table 1 and Figure 3A). The outstanding question raised by this proton movement is the correct Glu-402 ionization state. Does the glutamate side chain remain protonated and engage Cys-99 thiolate as the neutral carboxylic acid, or is its proton lost to solvent? A powerful argument for a neutral Glu-402 carboxylic acid is the observed closeness of the Cys-99 and Glu-402 pair (S···Oϵ distance of 2.95 Å). QM/MM geometry optimization of an ionized Glu-402 along with an ionized Cys-99 structure indicates that electrostatic repulsion would lead to a larger separation (S···Oϵ distance of 3.6 Å), not seen by the experimental data.

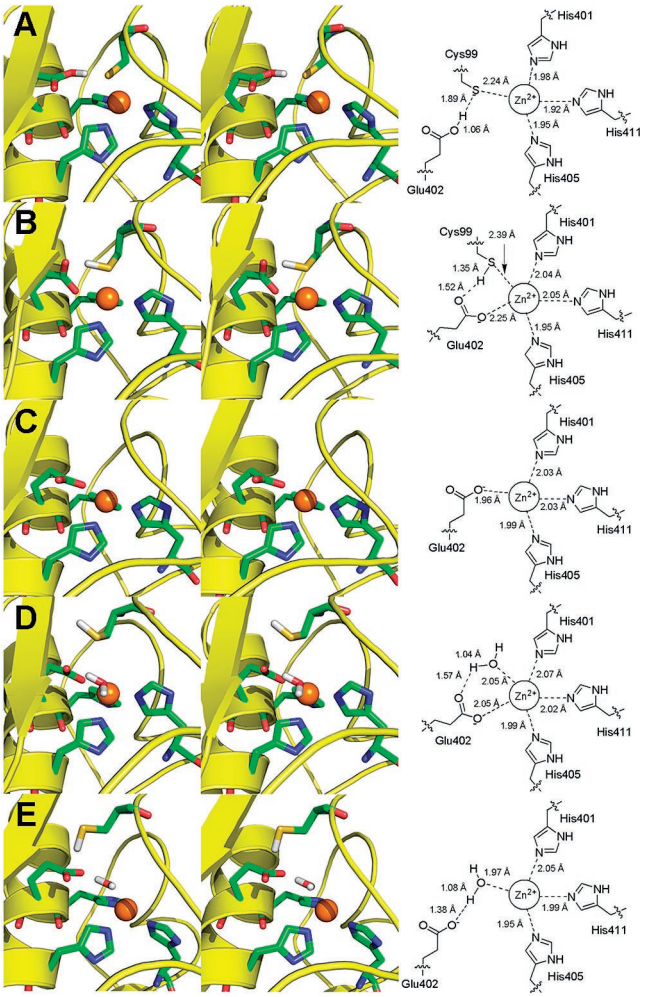

Figure 3. MMP-9 active-site structures of the intermediates in the activation process, as identified by QM/MM computation. The intermediates are shown as 3D (left panel) and 2D representations (right panel). (A) pro-MMP-9. (B) Intermediate **I-1**. (C) Intermediate **I-2**. (D) Intermediate **I-3**. (E) Active species. The protein is depicted in yellow ribbon, and the individual residues are depicted in capped sticks representation using atom coloring of C (green), N (blue), O (red), and S (yellow). The Zn atom is depicted as the orange sphere. See also MPEG animation in Supporting Information video 1.

The calculations show that the proton resides on Glu402 in the zymogen. However, changes in the active-site microenvironment are likely to happen gradually over the course of activation, and thus it should indeed be the case that the proton transfer back to Cys99 would occur over several incremental displacements that correspond to local energy minima. These intermediate states, however, were not observed in our calculations, as the focus was entirely on either the reactant or the product of the proton-transfer event.

The first intermediate (**I-1**) seen by XAS is a pentacoordinated zinc with one S and four N/O ligands. The most likely identity for the oxygen atom is the side chain of Glu-402, which is 4.3

(55) Kotra, L. P.; Cross, J. B.; Shimura, Y.; Fridman, R.; Schlegel, H. B.; Mobashery, S. *J. Am. Chem. Soc.* **2001**, *123*, 3108−3113.

Å from the zinc ion in the pro-MMP-9 crystal structure. MD simulation of the zymogen structure shows the ability of Oϵ of the Glu-402 carboxylic acid to approach within 3 Å of the zinc ion. A snapshot of this proximal Glu-402 structure was optimized using QM/MM. The result was Glu-402 reversion to the starting tetracoordinated zinc. Hence, a neutral carboxylic acid Glu-402 may approach, but cannot enter, into zinc coordination (as is necessary to account for **I-1**). The alternative explanation is that only when Glu-402 is an ionized carboxylate, such as would occur by back proton transfer to Cys-99, is it capable of entering into zinc coordination. A reasonable provocation for this proton transfer, as the initiating event in zymogen maturation, is formation of the tissue kallikrein−pro-MMP-9 complex.

MD simulation of the Glu-402 carboxylate and neutral Cys-99 thiol pair identified the probable transition of the zymogen conformer to **I-1**. The side chain of Glu-402 rotates 90° about its Cγ−Cδ bond, resulting in coordination of one carboxylate oxygen to the zinc ion and formation of a hydrogen bond to Cys-99 through the other oxygen (Figure 3B). The Zn−S and Zn−O bond lengths from QM/MM geometry optimization of this conformer are 2.39 and 2.25 Å, respectively. The Zn−N distances are 1.95, 2.04, and 2.05 Å. These results are comparable to the experimental bond lengths for **I-1** (Table 1).

Progression of the MD simulation beyond **I-1** reveals a small conformational change by Cys-99, accomplished by rotation around its Cα−Cβ bond and resulting in the Sγ−Hγ bond pointing away from Glu-402 and toward the backbone carbonyl oxygen of Cys-99 (Figure 3C). QM/MM geometry optimization of this intermediate confirmed that Cys-99 had dissociated from the first coordination shell of the zinc ion, giving a tetrahedral zinc showing coordination by Glu-402 and the three histidines. This species corresponds to **I-2**. The Zn−ligand distances (Zn−O: 1.96 Å; Zn−N: 1.99, 2.03, 2.03 Å) are in good agreement with the experimental data for **I-2** (Table 1).

A remarkable event is observed following formation of **I-2** during the MD simulation: A water molecule from the bulk solvent, that had forged its way to a location near the active site, enters into zinc ion coordination. This event is accompanied by a large swinging motion of Cys-99 away from the S1 pocket toward Glu-402, resulting in a Zn−S distance exceeding 4.0 Å (Figure 3D). Hence, this conformer likely corresponds to the pentacoordinated species **I-3** detected in the XAS experiment. This structure was geometry-optimized by QM/MM to give distances (water: 2.05 Å; Glu-402: 2.05 Å; Zn−N: 1.99, 2.02, 2.07 Å) that are in good agreement with experiment (Table 1).

The final step is the transformation of **I-3** to the mature zinc coordination of MMP-9. This transformation is vividly revealed by MD simulation (Supporting Information video 1), showing Glu-402 dissociating from the Zn ion concomitant with a conformational change of the Zn-coordinated water molecule that forms a hydrogen bond with Glu-402 as it coordinates with the zinc ion. Both the 2 Å resolution crystal structure of an active MMP protein with a zinc-bound water[56] and the XAS data indicate that the zinc ion of the mature MMP is tetrahedral with one water and three histidine ligands. QM/MM geometry optimization of a snapshot collected from the MD simulation gave a Zn−O distance (1.97 Å) in good agreement with the crystal structure (2.03 Å) and with XAS (1.89 Å) values. It is of interest to note that, following the geometry optimization, no proton migration from water to the Oϵ of Glu-402 was observed. The large dielectric constant that will result from the direct exposure of the active site to solvent at this stage, as is the case for the active MMP, will reduce the pK_a of Glu-402 and prevent proton transfer from water. This is distinct from what is seen for the zymogen (Figure 3A) where the lack of solvent, and hence low dielectric, favors proton transfer from Cys-99 to Glu-402.

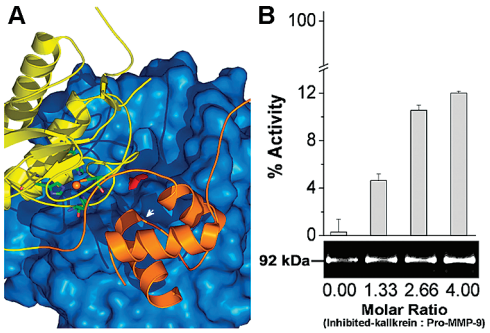

Figure 4. Zymogen activation is triggered by protein−protein interactions. (A) Proposed model of the complex between tissue kallikrein (shown in blue surface) and pro-MMP-9. The catalytic domain of pro-MMP-9 is shown in yellow (the catalytic zinc is shown as an orange sphere), and the pro-peptide domain is in orange ribbon. The residues coordinated to this zinc are shown in capped sticks representation with atom coloring of C (green), N (blue), O (red), and S (yellow). The model for the complex was obtained by docking the crystal structures of pro-MMP-9 and tissue kallikrein[54,59] using 3D-Dock.[34] In this model, the catalytic Ser-195 residue of tissue kallikrein (shown as red patch) is 14.7 Å away from the Leu-78 residue of the first cleavage site of pro-MMP-9 (see arrow). This suggests that protein conformational transitions at the pro-peptide domain are required for effective cleavage. (B) Incubation of pro-MMP-9 with various concentrations of irreversibly inhibited tissue kallikrein. Increased catalytic ability of MMP-9 for peptide hydrolysis activity as measured by gel zymography (lower panel) and fluorescent substrate hydrolysis (upper panel) assays, while the pro-domain remains intact (lower panel). This indicates that "cysteine switch" is induced by protein−protein interactions (using inhibited kallikrein) without proteolytic loss of the pro-peptide domain. The maximal rate of peptide hydrolysis (12% relative to the value obtained by active kallikrein MMP-9 activation, Figure 1B) indicates that dissociation of the pro-peptide domain is required for full MMP activity.

"Cysteine Switch" Is Triggered by Protein−Protein Interactions. Our results provide a detailed explanation of the activation events for the MMP-9 zymogen. Using stopped-flow XAS, we show that dissociation of the conserved pro-MMP-9 cysteine ligand from the zinc ion occurs at the earliest stages of the activation reaction, during interaction with the activator protease and in the absence of significant proteolysis. The key event in the maturation of the zinc coordination, subsequent to this protease binding to the "bait" domain, is suggested as proton transfer within the Glu-Cys dyad, as was surmised previously.[55] Computational docking of tissue kallikrein with pro-MMP-9 (see Materials and Methods) suggests that protein conformational transitions, which result in the relaxation of the pro-domain, must occur to facilitate the hydrolytic steps since the first proteolytic cleavage site of the pro-domain is distant from the catalytic site of tissue kallikrein (Figure 4A and Supporting Information Figure S2). Remarkably, incubation of MMP-9 zymogen with increasing amounts of *inactive* tissue kallikrein (as a result of inhibition by the active-site covalent modifier phenylmethylsulphonyl fluoride)[57] resulted in moderate levels of MMP-9 activity (as discerned by the use of a peptide

(56) Chen, L.; Rydel, T. J.; Gu, F.; Dunaway, C. M.; Pikul, S.; Dunham, K. M.; Barnett, B. L. *J. Mol. Biol.* **1999**, *293*, 545−557.

substrate) while the enzyme pro-peptide domain remained covalently intact (Figure 4B). Incubation of pro-MMP-9 with BSA (an unrelated protein, serving as a control) resulted in no detectable activation of pro-MMP-9 (data not shown), suggesting that particular protein−protein interactions are required to achieve activation. This suggests that the "cysteine switch" process at the catalytic zinc ion is triggered by zymogen-activator complexation, and hence protein−protein interactions are followed by conformational transition of the pro-peptide domain to allow effective hydrolytic cleavage. Interestingly, Bannikov et al. reported that MMP-9 zymogen−gelatin interactions induced pro-peptide domain disengagement.[58] The results reported herein provide the molecular and structural means for this remarkable observation.

Conclusions

It is now recognized that triggering of MMP activity goes beyond their role in matrix remodeling[1,59] Upon activation, MMPs interact with a variety of bioactive molecules to promote signaling circuits and regulation of systemic and interstitial environments. This work provides the first mechanistic understanding of the dynamic atomic events leading to activation of pro-MMP-9. Our work provides novel experimental evidence to the long sought role of protein intradomain communication in mediating catalysis. Significantly, here we demonstrate the synergism among long-range protein conformational transitions, local structural rearrangements, and fine atomic events in the process of zymogen activation. Owing to the great structural similarity of MMP members,[60] this mechanism is likely relevant to all members of the MMP family[61] and might generally be relevant to the estimated 397 zinc-dependent hydrolases found in the human genome, many of which experience proteolytic activation mechanisms similar to what is disclosed in this report.[62]

Acknowledgment. We thank Dr. Marcos Milla (Roche, Palo-Alto) and Prof. Anatoly Frenkel (Yeshiva University) for critically reading this manuscript. This work was supported by grants from Minerva Foundation, Israel Science Foundation, the Clotide and Mauricio Pontecorvo Funds, and by a research grant from Mr. and Mrs. Michael Ambach to I.S. The work at the University of Notre Dame was supported by the National Institutes of Health.

Supporting Information Available: Supporting methods: Zinc content determination, N-terminal sequencing, protein−protein docking, detailed time-resolved XAS fitting results, MPEG animation, and full Gaussian 2003 citation. This material is available free of charge via the Internet at http://pubs.acs.org.

JA073941L

(57) Schmidt, A.; Jelsch, C.; Ostergaard, P.; Rypniewski, W.; Lamzin, V. S. *J. Biol. Chem.* **2003**, *278*, 43357−43362.
(58) Bannikov, G. A.; Karelina, T. V.; Collier, I. E.; Marmer, B. L.; Goldberg, G. I. *J. Biol. Chem.* **2002**, *277*, 16022−16027.
(59) Overall, C. M. *Biochem. J.* **2004**, *383*, e5−7.
(60) Maskos, K. *Biochimie* **2005**, *87*, 249−263.
(61) Milla, M.; Gonzales, P.; Leonard, J. *Cell Biochem. Biophys.* **2006**, *44*, 342−348.
(62) Andreini, C.; Banci, L.; Bertini, I.; Rosato, A. *J. Proteome Res.* **2006**, *5*, 196−201.
(63) Frisch, M. J., et al. Gaussian, Inc.: Pittsburgh, PA, 2003.